

# Electronic Supplementary Information

## Probing weak non-covalent interactions in solution and solid states with designed molecules

Abil E. Aliev,\* Joëlle Moïse, William B. Motherwell,\* Miloslav Nič, Denis Courtier-Murias and Derek A. Tocher

### Contents

<b>Calculations</b>	<b>S2</b>
<b>NMR Measurements</b>	<b>S2</b>
<b>The temperature dependence of conformational populations of 1 in toluene</b>	<b>S3</b>
<b>Identification of conformers by NMR</b>	<b>S3</b>
<b>Populations of endo/exo conformers in solutions</b>	<b>S9</b>
<b>Crystallographic data</b>	<b>S11</b>
<b>QM/MD simulations of 1</b>	<b>S11</b>
<b>References</b>	<b>S13</b>

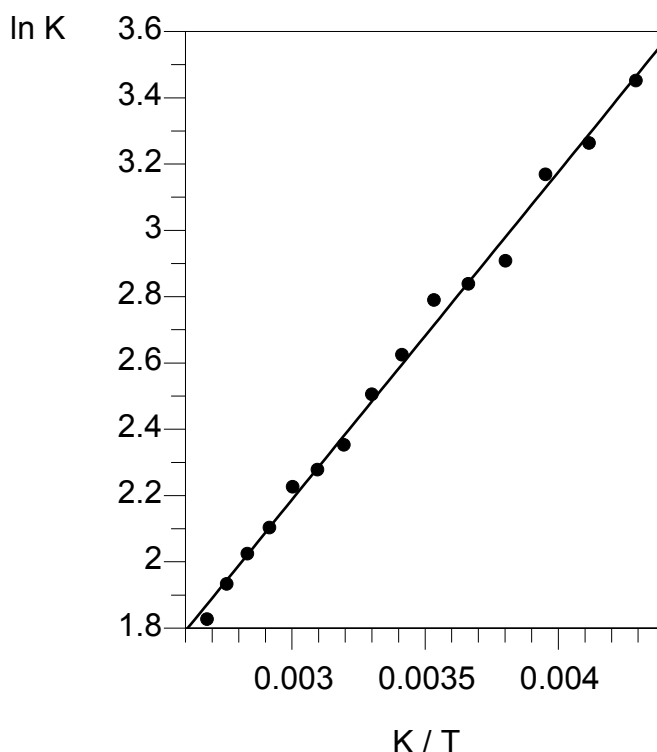
## Calculations

Force field and DFT calculations were carried out using PCMODEL<sup>[1]</sup> and Gaussian 03.<sup>[2]</sup> Geometry optimisations were done using either B3LYP/6-31G(d) or B3LYP/6-31+G(d) levels of theory. Solution state calculations used IEFPCM model,<sup>[3]</sup> as implemented in Gaussian 03. <sup>1</sup>H and <sup>13</sup>C NMR chemical shifts relative to TMS were computed at B3LYP/6-311+G(2d,p) level, whereas vibrational frequencies were calculated at the B3LYP/6-31G(d) level, using scaling factors of 0.9613.<sup>[4]</sup> The overall rms error for the frequency calculations by B3LYP/6-31G(d) has been reported to be 34 cm<sup>-1</sup>.<sup>[4]</sup>

## NMR Measurements

Solution <sup>1</sup>H and <sup>13</sup>C NMR spectra were recorded on Bruker NMR spectrometers AMX300, AMX400 and AVANCE500. <sup>1</sup>H and <sup>13</sup>C chemical shifts are given relative to TMS. Unless otherwise specified, spectra were recorded at 298 K. Selective NOE and 2D experiments were measured using AVANCE500, equipped with z-gradient facilities.

Solid-state <sup>13</sup>C spectra were recorded at 75.5 MHz and 30.1 MHz, respectively, using a standard 7 mm double-resonance magic-angle spinning (MAS) probe on MSL300 (Bruker). Samples in zirconia rotors of 7 mm external diameter were spun at 4-5 kHz with stability better than ±3 Hz. Spectra were recorded using cross-polarization (CP), MAS and high-power <sup>1</sup>H decoupling. Dipolar-dephased CPMAS NMR spectra were also acquired. <sup>13</sup>C chemical shifts are reported relative to TMS and solid adamantane (29.47 ppm, CH) was used as external chemical shift reference.

**The temperature dependence of conformational populations of **1** in toluene**

**Figure S1.** The temperature dependence of the equilibrium constant,  $K=x^{\text{endo}}/x^{\text{exo}}$ , for **1** in toluene- $d_8$ . From the linear dependence of  $\ln K$  vs.  $T^{-1}$ , the enthalpy and entropy terms in the free energy expression can be determined as  $\Delta H^\circ = -(8.2 \pm 0.2) \text{ kJ mol}^{-1}$  and  $\Delta S^\circ = -(6.5 \pm 0.6) \text{ J K}^{-1} \text{ mol}^{-1}$  ( $r = 0.997$ )

**Identification of conformers by NMR**

The major conformers were determined using a series of selective NOE experiments,<sup>[5]</sup> as well as  $^1J_{\text{CH}}$  and  $^3J_{\text{CH}}$  coupling measurements. An example of NOE experiment is shown in Figure S2. Here, methyl protons were selectively excited and the enhancement ratio for protons H<sub>A</sub> and H<sub>B</sub> ( $\eta_A/\eta_B$ ) was found to be 1.73 (see Figure S3 for proton numbering).

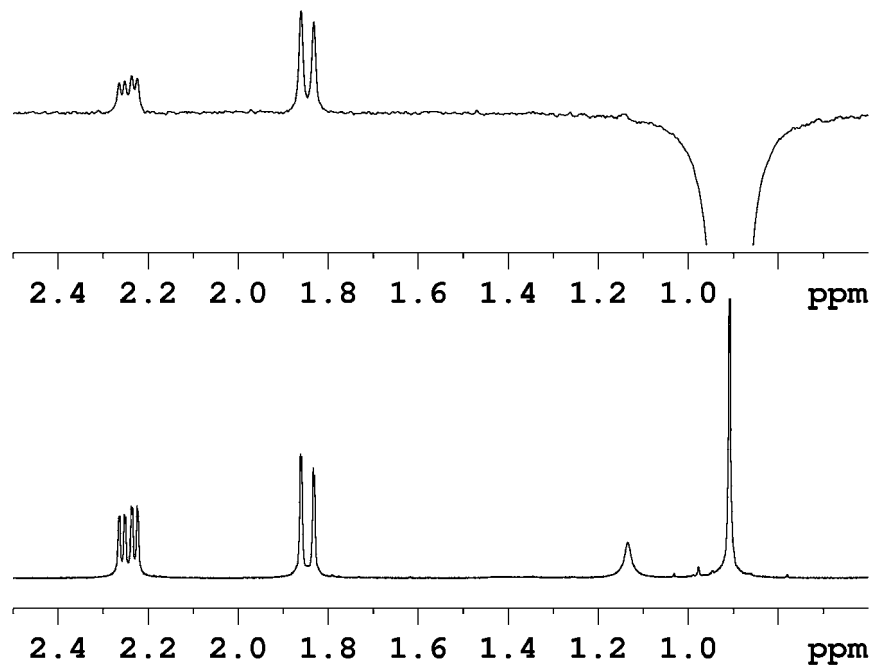


**Figure S2.** Top: selective NOE spectrum of **1** in  $C_6D_6$  (with 1 Hz line broadening). Bottom: static <sup>1</sup>H NMR spectrum of **1** in  $C_6D_6$  (no line broadening).

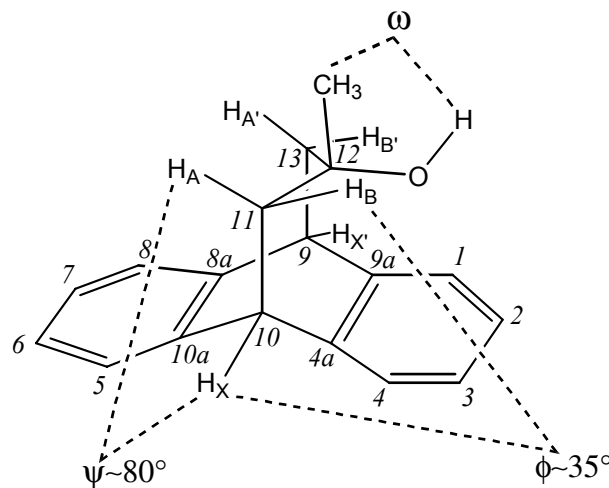
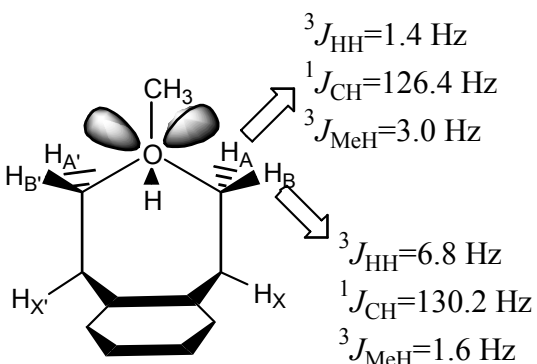


**Figure S3.** Definition of dihedral angles and atom numbering illustrated for **1**.

On a qualitative level, higher enhancement observed for proton  $H_A$  is in favour of the O-endo conformation. A more detailed consideration of the enhancements observed requires accounting for fast methyl group rotation, which leads to a motional averaging of methyl protons with the averaged position (denoted as  $Me^*$ ) along the  $C_{12}-C_{12'}$  direction. From the gas phase B3LYP/6-31G(d) optimised geometries, distances  $C_{12'}-H_A$  and  $C_{12'}-H_B$  were 2.606 Å and 2.803 Å, respectively, in the O-endo conformation of **1**. These distances, together with the corresponding angles were used to

determine internuclear distances,  $r$ , for H<sub>A</sub>,Me\* (2.828 Å) and H<sub>B</sub>,Me\* (3.063 Å) pairs. Thus, using the initial rate approximation,<sup>[6]</sup> which is based on the  $r^{-6}$  dependence of NOEs, the expected enhancement ratio is 1.62. This compares well with the measured value of 1.71. For comparison, in the alternative O-exo conformation the value of  $\eta_A/\eta_B$  is 0.20, which is significantly different from the value for the O-endo form. Measurements in CDCl<sub>3</sub> at 263 K resulted in the observed ratio of 1.63. Furthermore, unlike Me protons, no positional averaging is present for proton H<sub>X</sub>, hence the NOE experiment with selective excitation of H<sub>X</sub> was used as a control for the above approach, as well as for examining the significance of the zero-quantum coherence effects.<sup>[6]</sup> For the CDCl<sub>3</sub> solution of **1** at 263 K, the predicted and the observed enhancement ratios  $\eta_A/\eta_B$  were 1.67 and 1.66, respectively.

In some cases, a pair of direct  $^1J_{CH}$  couplings of 11(13)-CH<sub>2</sub> (Figure S3) was also used for the determination of the preferred orientation of the substituents at C<sub>12</sub>. Here we use the well-known dependence of the  $^1J_{CH}$  couplings on the proximity of the electron lone pairs.<sup>[7]</sup> For example, the H<sub>B</sub> proton is expected to show a higher value of  $^1J_{CH}$  due to its vicinity to the oxygen lone pairs in the O-endo conformation of **1**:



For the alternative O-exo conformation all methylene protons are *gauche* relative to oxygen, hence approximately equal  $^1J_{CH}$  couplings are expected. The measured values of  $^1J_{CH}$  (in CDCl<sub>3</sub> at 298 K) are shown in the scheme above. In addition, the well-known Karplus dependence of the  $^3J_{CH}$  couplings<sup>[7]</sup> suggests that for the methyl carbon two relatively small couplings with protons H<sub>A</sub> and H<sub>B</sub> are expected, since corresponding dihedral angles with protons H<sub>A</sub> and H<sub>B</sub> are approximately 40° and 75°, respectively. Measurements of direct and vicinal  $^{13}C$ - $^1H$  couplings were particularly useful

in the case of epoxide **2**, as small chemical shift differences between the protons of interest were observed, making the use of NOEs less efficient for **2**. Details of NMR analysis for this compound combined with the B3LYP geometries are included in Figure S4. Similarly, the vicinal  $^{13}\text{C}$ - $^1\text{H}$  couplings of the CN carbons with protons  $\text{H}_\text{A}$  and  $\text{H}_\text{B}$  were used for the determination of the preferred orientation of the substituents at  $\text{C}_{12}$  in **4** and **6**.

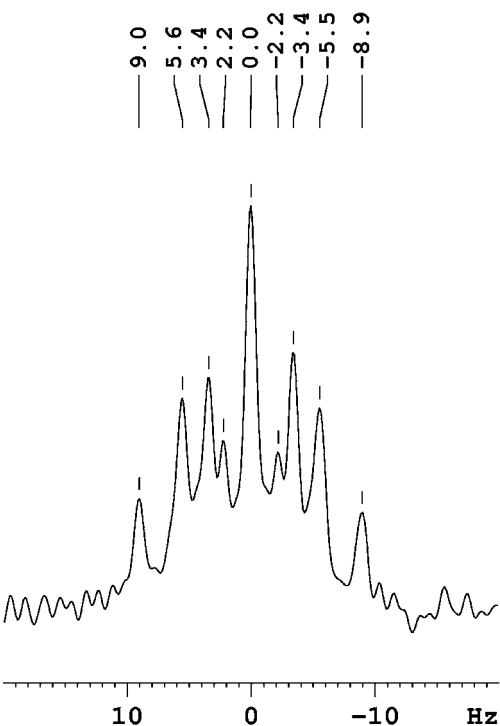
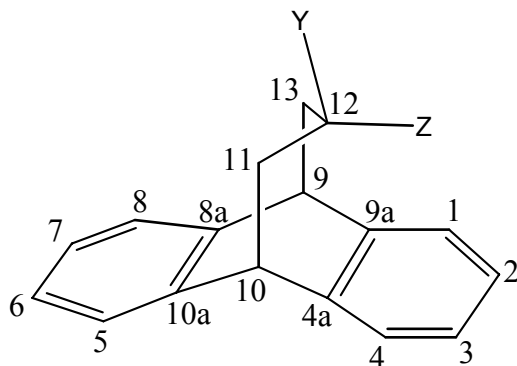


**Figure S4.** Proton-coupled  $^{13}\text{C}$  spectrum of epoxide **2** in  $\text{C}_6\text{D}_6$ . The multiplicity of the central peak of the epoxide methylene carbon due to the  $^3J_{\text{CH}}$  couplings is shown. The measured values were:  $^3J(\text{C}_{12}, \text{H}_\text{B})=5.5$  Hz and  $^3J(\text{C}_{12}, \text{H}_\text{B})=3.4$  Hz. Corresponding dihedral angles,  $\theta$ , measured from the B3LYP 6-31G(d) optimised geometries were  $15^\circ$  and  $131^\circ$  ( $17^\circ$  and  $134^\circ$  from crystallographic measurements), respectively, in the O-exo conformer and  $39^\circ$  and  $77^\circ$  in the O-endo conformer. Based on the Karplus relationship,<sup>[7]</sup> the measured values are in favour of the major O-exo conformer. In the DMSO- $d_6$  solution at 298 K, with  $^3J(\text{C}_{12}, \text{H}_\text{B})=4.9$  Hz and  $^3J(\text{C}_{12}, \text{H}_\text{B})=3.4$  Hz, the O-exo conformer is also the major form. The smaller value of  $^3J(\text{C}_{12}, \text{H}_\text{B})$  indicates a decrease of the O-exo population compared to the benzene solution, whereas no change of  $^3J(\text{C}_{12}, \text{H}_\text{B})$  is the consequence of the boundary dihedral angle values in the O-exo ( $131^\circ$ ) and O-endo ( $39^\circ$ ) conformers, which correspond to approximately equal  $J$ -couplings on the Karplus curve.

Finally,  $^1\text{H}$  and  $^{13}\text{C}$  chemical shifts of **1** and **6** were calculated using B3LYP 6-311+G(2d,p) (Tables S1 and S2). A significantly better agreement was found for the  $^1\text{H}$  chemical shifts compared to the  $^{13}\text{C}$  chemical shifts when comparing experimentally measured values and calculated values for the O-endo conformation of **1**.

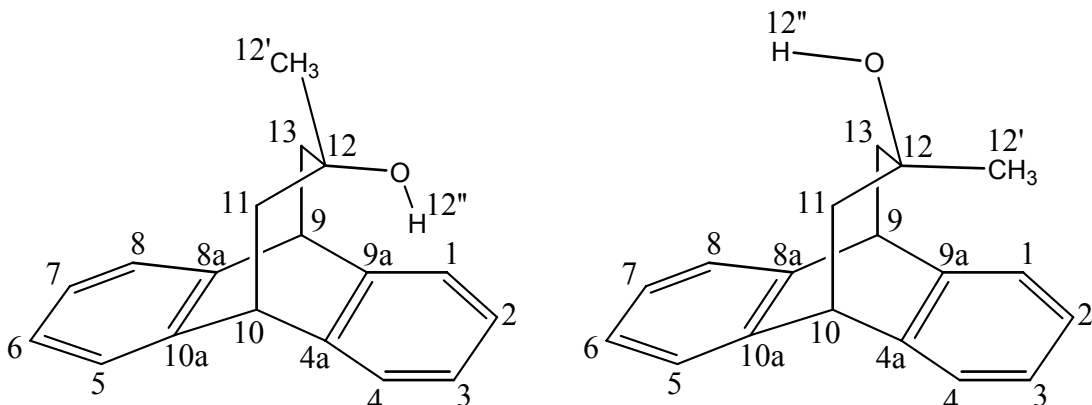
**Table S1.**  $^{13}\text{C}$  NMR chemical shifts in the solid-state (SS) and in  $\text{CDCl}_3$ . DFT B3LYP/6-311G(2d,p)//B3LYP/6-31G(d) chemical shifts of **6** are also included.



Carbon	<b>1</b> in $\text{CDCl}_3$	<b>1</b> SS	<b>2</b> in $\text{CDCl}_3$	<b>4</b> in $\text{CDCl}_3$	<b>6</b> in $\text{CDCl}_3$	<b>6</b> SS	<b>6</b> DFT
1,4	126.4	125.2-128.5	126.6-125.7	127.1	127.0	124-131	132.1
2,3	126.9	125.2-128.5	126.6-125.7	127.4	127.5	124-131	132.1
5,8	125.2	125.2-128.5	126.6-125.7	125.8	125.5	124-131	130.0
6,7	126.2	125.2-128.5	126.6-125.7	126.6	126.8	124-131	132.0
4a,9a	141.6	141.5 142.3 142.6 142.8	142.3	140.2	139.6	140.4 141.3	147.5
8a,10a	144.2	145.4 146.5 147.2 147.2	143.0	142.5	143.5	142.9 143.7	152.4
9,10	44.9	45.9 46.4	44.7	43.3	43.8	42.9 43.6	51.3
11,13	44.6	42.6 44.1 44.4 45.4	41.0	42.2	41.7	41.2 42.0	45.2
12	72.7	71.7 73.1	56.8	69.5	50.6	51.1 52.0	55.0
12'	32.8	33.8 34.5	54.7	121.4	123.9	127.5 <sup>a</sup> 127.9 <sup>a</sup>	130.8
			-				

<sup>a</sup>Two peaks for the cyano carbon are due to the ( $^{13}\text{C}$ ,  $^{14}\text{N}$ ) residual dipolar coupling.

**Table S2.** Experimental (in  $\text{CDCl}_3$  and  $\text{C}_6\text{D}_{12}$  at 298K) and calculated chemical shifts (in gas phase and in cyclohexane) of alcohol **1** relative to TMS using B3LYP/6-311+G(2d,p) level of theory and B3LYP/6-31G(d) optimised geometries. Averaged calculated values are given in the case of rotameric inequivalence.



O-endo

O-exo

Atom	$\delta_{\text{C}}^{\text{calc}}$ /ppm O-endo ( <i>trans/gauche</i> )	$\delta_{\text{C}}^{\text{exp}}$ /ppm $\text{CDCl}_3$	$\delta_{\text{C}}^{\text{calc}}$ /ppm O-exo ( <i>trans/gauche</i> )	$\delta_{\text{H}}^{\text{calc}}$ /ppm O-endo ( <i>trans/gauche</i> )	$\delta_{\text{H}}^{\text{exp}}$ /ppm $\text{CDCl}_3/\text{C}_6\text{D}_{12}$	$\delta_{\text{H}}^{\text{calc}}$ /ppm in cyclohexane, O-endo ( <i>trans/gauche</i> )
1,4	131.6 / 130.2	126.4	131.4 / 130.8	7.65 / 7.45	7.37 / 7.22	7.75 / 7.54
2,3	132.5 / 131.2	126.9	131.7 / 131.8	7.51 / 7.35	7.22 / 7.08	7.59 / 7.43
5,8	130.3 / 130.2	125.2	129.6 / 130.2	7.49 / 7.51	7.26 / 7.11	7.63 / 7.61
6,7	131.3 / 131.2	126.2	131.8 / 131.4	7.40 / 7.37	7.15 / 7.01	7.49 / 7.47
4a,9a	150.4 / 150.0	141.6	149.2 / 149.8	-	-	-
8a,10a	152.4 / 152.7	144.2	152.7 / 152.5	-	-	-
9,10	52.9 / 52.8	44.9	52.5 / 52.3	4.07 / 4.03	4.12 / 3.96	4.14
11,13	49.4 / 47.8	44.6	52.0 / 48.2	1.91 / 1.82 ( $\text{H}_A$ ) 2.36 / 2.06 ( $\text{H}_B$ )	1.93 / 1.84 ( $\text{H}_A$ ) 2.30 / 2.21 ( $\text{H}_B$ )	1.93 / 1.82 ( $\text{H}_A$ ) 2.37 / 2.10( $\text{H}_B$ )
12	78.0 / 78.4	72.7	77.4 / 77.5	-	-	-
12'	33.7 / 37.0	32.8	31.5 / 36.5	0.85 / 0.89	0.93 / 0.81	0.85 / 0.89
12''	-	-	-	0.63 / -1.06	1.14 / 0.79	0.71 / -0.56

# Supplementary Material (ESI) for PCCP

# This journal is (c) The Owner Societies 2008

## Populations of endo/exo conformers in solutions

As the interconversion barrier of the bridged bicyclic 9,10-propanoanthracenes is very low, an alternative approach was used based on the fact that equilibrium constants can be calculated using the observed averaged coupling constants if the  $J$ -couplings in both conformers are known. The temperature and solvent dependences of the conformer populations proved useful for the evaluation of the boundary  ${}^3J_{\text{HH}}$  values. In addition, advantage was taken of the fact that we had a series of similar compounds with varying conformational preferences, which would allow a reasonable estimate to be made. Despite its indirect nature, an advantage of the  ${}^3J_{\text{HH}}$ -based approach, especially in the case of temperature dependent population changes, is that conformer population ratios for **1-6** with different functional groups can be compared at the same temperature (Table S3).

In the case of two-site equilibrium, the populations (in %) of the O(N)-endo and O(N)-exo conformations ( $x^{\text{endo}}$  and  $x^{\text{exo}}=100-x^{\text{exo}}$ ) can be calculated using:

$$\bar{J} = (J^{\text{endo}} x^{\text{endo}} + J^{\text{exo}} x^{\text{exo}}) / 100$$

where  $\bar{J}$  is the measured averaged coupling constant (either  ${}^3\bar{J}_{AX}$  or  ${}^3\bar{J}_{BX}$ ) whereas  $J^{\text{endo}}$  and  $J^{\text{exo}}$  are corresponding boundary vicinal couplings in conformers O(N)-endo and O(N)-exo, respectively.

Since some assumptions in the estimation of the boundary coupling constants had to be made, a realistic estimate of the introduced error is of importance. Possible errors may follow from the fact that the degree of twisting of the bridge in different compounds and conformations may differ and that electronic characteristics of the functional groups may influence the coupling constants of their neighbours. In order to assess magnitude of these factors corresponding dihedral angles in both conformers of various bicyclononanes were calculated. The geometries from various force-field and DFT calculations did not indicate any significant changes of dihedral angles  $\phi$  and  $\psi$  that would be critical for  ${}^3J_{\text{HH}}$ -analysis. The overall ranges of torsion changes on using different force fields (MMX, AMBER and OPLSA) and B3LYP/6-31G(d) were 32-42° and 75-81°, respectively.

In addition to the above, we note that the present system provide an internal check inasmuch as the sum of the measured couplings  ${}^3\bar{J}_{AX}$  and  ${}^3\bar{J}_{BX}$  were approximately the same for the series, within  $\pm 3\%$  for the disubstituted derivatives (Table S3). This is a consequence of the fact that the changes in substituent electronegativities, as well as their orientation relative to the coupled proton pairs have only small effect for a given series of compounds. A similar relationship was also found for calculated  ${}^3J_{HH}$  couplings on using optimised molecular geometries and modified Karplus equation by Haasnoot *et al.*<sup>[8]</sup> The latter accounts for the dependence of  ${}^3J_{HH}$  on both dihedral angle and substituent electronegativities. Overall, this type of *J*-coupling predictions, rather than explicit calculations by ab initio or DFT methods proved useful.

**Table S3.** Population ratios and free energy differences between O(N)-endo and O(N)-exo conformers from  ${}^3J_{HH}$  in C<sub>6</sub>D<sub>6</sub> at 298K. Boundary values used were 7.3 and 1.0 Hz. Assuming that the boundary  ${}^3J_{HH}$  values are accurate within  $\pm 0.3$  Hz, the error of population measurements is estimated as  $\pm 5\%$ .

Compound	${}^3\bar{J}_{BC}$ / Hz	${}^3\bar{J}_{AC}$ / Hz	$x^{\text{endo}} : x^{\text{exo}}$	$\Delta G^\circ$ <sup>a</sup> / kJ mol <sup>-1</sup>
<b>1</b>	6.5	1.7	89:11	-5
<b>2</b>	2.6	5.7	25:75	3
<b>3</b>	1.3	7.1	5:95	7
<b>4</b>	2.4	5.7	24:76	3
<b>5</b>	5.6	2.7	73:27	-3
<b>6</b>	1.4	7.0	5:95	7

<sup>a</sup> The free energy difference,  $\Delta G^\circ$ , is defined such that a negative value corresponds to a more stable O(N)-endo conformation [ $\Delta G^\circ = -RT \ln(x^{\text{endo}}/x^{\text{exo}})$ ].

## Crystallographic data

The CIF files for epoxide **2** (sse0583.cif, prepared by the EPSRC National Crystallographic Service the SRS facility in Daresbury, Prof. W. Clegg, University of New Castle) and  $\alpha$ -amino nitrile **6** (str0215.cif) are provided as separate files for further visualization/processing purposes. These files also include details of crystallographic measurements.

## QM/MD simulations of **1**

Semi-empirical QM/MD simulations with the "standard" pairwise generalised Born solvation model for implicit solvent simulations<sup>[13]</sup> in cyclohexane were carried out for a system containing 1 molecule of **1**. These calculations were performed with the PM3 level of theory<sup>[14]</sup> for **1** using SANDER of AMBER 9.<sup>[15]</sup> The MD simulations were of the *NVT*-type and the temperature was controlled to 300 K with the Langevin algorithm using an isotropic position scaling with a 2 ps time constant. The nonbonded cut-off distance was set to 12.0 Å. After a minimisation step and an equilibration over 400 ps, production runs were executed for 10 ns with a time step of 2 fs and for 1 ns with a time step of 0.2 fs.

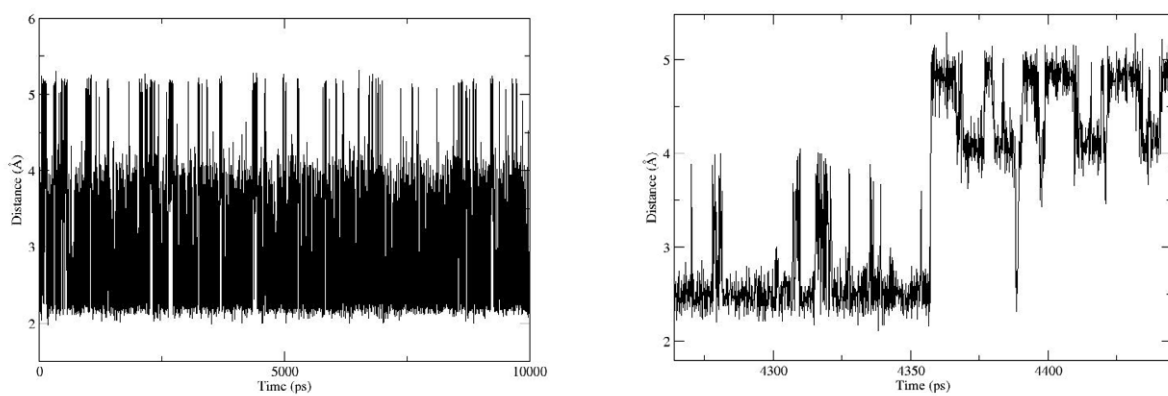


**Figure S5.** The change of the average distance between the hydroxyl proton and the two nearest quaternary aromatic carbons in the O-endo conformer as a function of time over 10 ns MD run (left) together with the expansion of the region near 4.4 ns (right).

The time dependence of the average distance between the hydroxyl proton and the two nearest quaternary aromatic carbons in the O-endo conformer as a function of time over 10 ns MD run is shown in Figure S5. As can be seen from this figure, there is a large number of conformational transitions over 10 ns long MD calculations, i.e., lifetime of a given conformational state is of the order of several picoseconds. For example, from the expansion showing in Figure S5 (right), the longest time the molecule spends in one state can be estimated to be less than 40 ps (near  $t=4.3$  ns). For comparison, this time period was ca. 3.4 ns in a similar type of calculation with SCC-DFTB<sup>[16]</sup> instead of PM3. Hence the relatively short length of the MD run (10 ns) is sufficient on using the PM3 method for estimating populations of different conformations, but not for the SCC-DFTB calculations.

The population distribution of the average distance between the hydroxyl proton and the two nearest quaternary aromatic carbons in the O-endo conformer is shown in Figures S6 and S7. From the integration of peaks in these figures, the populations ratio of four conformers *trans*-O-endo : *gauche*-O-endo : *gauche*-O-exo : *trans*-O-exo was estimated to be 11:1:1:1, which agrees well with the experimentally measured  $^3J_{\text{HH}}$  and  $^3J_{\text{CH}}$  couplings (see discussion and Table 1 the main text).

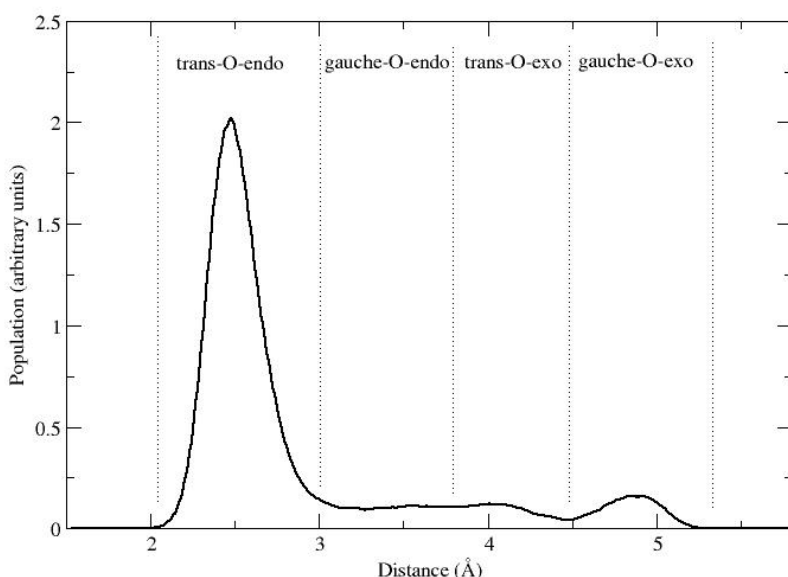


**Figure S6.** Distribution of conformers as a function of the average distance between the hydroxyl proton and the two nearest quaternary aromatic carbons in the O-endo conformer from PM3 MD calculations (duration 10 ns, timestep 2 fs).

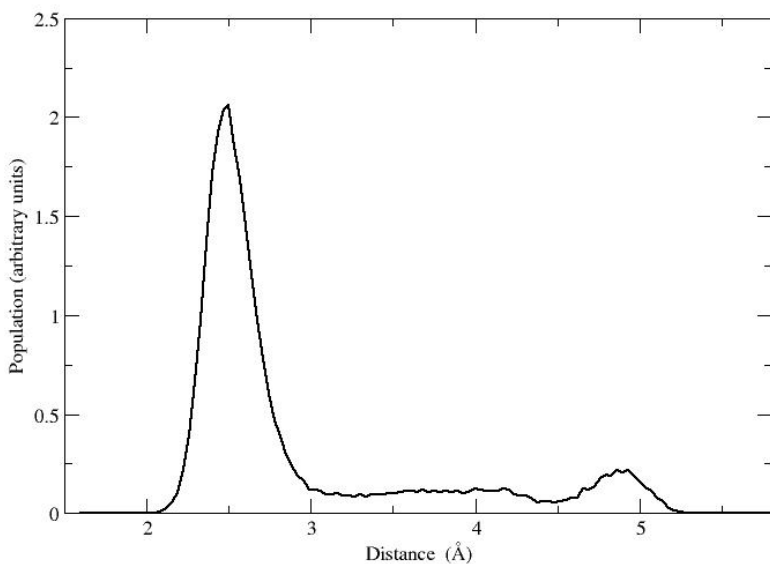


**Figure S7.** Distribution of conformers as a function of the average distance between the hydroxyl proton and the two nearest quaternary aromatic carbons in the O-endo conformer from PM3 MD calculations (duration 1 ns, timestep 0.2 fs).

Based on a similar type of population distribution curve for the average distance between the hydroxyl oxygen and the two nearest quaternary aromatic carbon, the population of the O-endo conformer was estimated to be 86%, which agrees well with the experimentally measured value of 93% in C<sub>6</sub>D<sub>12</sub> (Table 1, main text).

## References

1. PCMODEL (version 8.5, Serena Software). See also: M. F. Schlecht, Molecular Modeling on the PC, Wiley-VCH, New York, 1998.
2. Gaussian 03, Revision B.05, M. J. Frisch, G. W. Trucks, H. B. Schlegel, G. E. Scuseria, M. A. Robb, J. R. Cheeseman, J. A. Montgomery, Jr., T. Vreven, K. N. Kudin, J. C. Burant, J. M. Millam, S. S. Iyengar, J. Tomasi, V. Barone, B. Mennucci, M. Cossi, G. Scalmani, N. Rega, G. A. Petersson, H. Nakatsuji, M. Hada, M. Ehara, K. Toyota, R. Fukuda, J. Hasegawa, M. Ishida, T. Nakajima, Y. Honda, O. Kitao, H. Nakai, M. Klene, X. Li, J. E. Knox, H. P. Hratchian, J. B.

- Cross, V. Bakken, C. Adamo, J. Jaramillo, R. Gomperts, R. E. Stratmann, O. Yazyev, A. J. Austin, R. Cammi, C. Pomelli, J. W. Ochterski, P. Y. Ayala, K. Morokuma, G. A. Voth, P. Salvador, J. J. Dannenberg, V. G. Zakrzewski, S. Dapprich, A. D. Daniels, M. C. Strain, O. Farkas, D. K. Malick, A. D. Rabuck, K. Raghavachari, J. B. Foresman, J. V. Ortiz, Q. Cui, A. G. Baboul, S. Clifford, J. Cioslowski, B. B. Stefanov, G. Liu, A. Liashenko, P. Piskorz, I. Komaromi, R. L. Martin, D. J. Fox, T. Keith, M. A. Al-Laham, C. Y. Peng, A. Nanayakkara, M. Challacombe, P. M. W. Gill, B. Johnson, W. Chen, M. W. Wong, C. Gonzalez, and J. A. Pople, Gaussian, Inc., Wallingford CT, 2004.
3. E. Cancès and B. Mennucci, *J. Math. Chem.*, 1998, **23**, 309.
  4. M.W. Wong, *Chem. Phys. Lett.*, 1996, **256**, 391.
  5. J. Stonehouse, P. Adell, J. Keeler and A.J. Shaka. *J. Amer. Chem. Soc.*, 1994, **116**, 6037.
  6. D. Neuhaus and M.P. Williamson. The Nuclear Overhauser Effect in Structural and Conformational Analysis, 2nd Edition, Wiley-VCH, 2000.
  7. R.H. Contreras and J.E. Peralta, *Prog. Nucl. Magn. Reson.*, 2000, **37**, 321.
  8. C.A.G. Haasnoot, F.A.A.M. DeLeeuw and C. Altona, *Tetrahedron*, 1980, **36**, 2783.
  9. F. Weiss and R. Rusch, *Bull. Soc. Chim. Fr.*, 1964, 550.
  10. B. B. Snider, *J. Org. Chem.*, 1973, **38**, 3961.
  11. M. Nič, PhD Thesis, *University of London*, 1995.
  12. H. M. R. Hoffmann and U. Karama, *Chem. Ber.*, 1992, **125**, 2803.
  13. (a) V. Tsui, D.A. Case, *Biopolymers*, 2001, **56**, 275; (b) V. Tsui, D.A. Case, *J. Am. Chem. Soc.*, 2000, **122**, 2489; (c) E. Pellegrini, M. J. Field. *J. Phys. Chem. A.*, 2002, **106**, 1316.
  14. J.J.P. Stewart, *J. Comput. Chem.* 1989, **10**, 209.

15. D.A. Case, T.A. Darden, T.E. Cheatham, III, C.L. Simmerling, J. Wang, R.E. Duke, R. Luo, K.M. Merz, D.A. Pearlman, M. Crowley, R.C. Walker, W. Zhang, B. Wang, S. Hayik, A. Roitberg, G. Seabra, K.F. Wong, F. Paesani, X. Wu, S. Brozell, V. Tsui, H. Gohlke, L. Yang, C. Tan, J. Mongan, V. Hornak, G. Cui, P. Beroza, D.H. Mathews, C. Schafmeister, W.S. Ross, P.A. Kollman, *AMBER 9*, University of California, San Francisco, **2006**.
16. M. Elstner, *Theor. Chem. Acc.* 2006, **116**, 316 and references therein.